Prediction of a monolayer spin-spiral semiconductor: CoO with a honeycomb lattice

Jie Zhang(张杰), Shunuo Song(宋姝诺), Yan-Fang Zhang(张艳芳), Yu-Yang Zhang(张余洋), Sokrates T. Pantelides, and Shixuan Du(杜世萱)

Citation: Chin. Phys. B, 2023, 32 (**8**): 087508. DOI: 10.1088/1674-1056/acd923
Journal homepage: http://cpb.iphy.ac.cn; http://iopscience.iop.org/cpb

What follows is a list of articles you may be interested in

Magnetic ordering induced magnetodielectric effect in $Ho_2Cu_2O_5$ and $Yb_2Cu_2O_5$

Hao Jin(金昊), Shuai Huang(黄帅), Kai-Qi Wan(万凯奇), Chang-Ming Zhu(朱长明),Hai-Ou Wang(王海欧), Kun-Peng Su(苏昆朋), and De-Xuan Huo(霍德璇)

Chin. Phys. B, 2023, 32 (**6**): 067504. DOI: 10.1088/1674-1056/ac904a

Structural evolution-enabled $BiFeO_3$ modulated by strontium doping with enhanced dielectric, optical and superparamagneticproperties by a modified sol-gel method

Sharon V S, Veena Gopalan E, and Malini K A

Chin. Phys. B, 2023, 32 (**3**): 037504. DOI: 10.1088/1674-1056/ac785b

Charge-mediated voltage modulation of magnetism in $Hf_{0.5}Zr_{0.5}O_2$/Co multiferroic heterojunction

Jia Chen(陈佳), Peiyue Yu(于沛玥), Lei Zhao(赵磊), Yanru Li(李彦如), Meiyin Yang(杨美音), Jing Xu(许静), Jianfeng Gao(高建峰), Weibing Liu(刘卫兵), Junfeng Li(李俊峰), Wenwu Wang(王文武), Jin Kang(康劲), Weihai Bu(卜伟海), Kai Zheng(郑凯), Bingjun Yang(杨秉君), Lei Yue(岳磊), Chao Zuo(左超), Yan Cui(崔岩), and Jun Luo(罗军)

Chin. Phys. B, 2023, 32 (**2**): 027504. DOI: 10.1088/1674-1056/ac9a3b

Computational studies on magnetism and ferroelectricity

Ke Xu(徐可), Junsheng Feng(冯俊生), and Hongjun Xiang(向红军)

Chin. Phys. B, 2022, 31 (**9**): 097505. DOI: 10.1088/1674-1056/ac7b1b

Strain-mediated magnetoelectric control of tunneling magnetoresistance in magnetic tunneling junction/ferroelectric hybrid structures

Wenyu Huang(黄文宇), Cangmin Wang(王藏敏), Yichao Liu(刘艺超), Shaoting Wang(王绍庭), Weifeng Ge(葛威锋), Huaili Qiu(仇怀利), Yuanjun Yang(杨远俊), Ting Zhang(张霆), Hui Zhang(张汇), and Chen Gao(高琛)

Chin. Phys. B, 2022, 31 (**9**): 097502. DOI: 10.1088/1674-1056/ac523e

---

RAPID COMMUNICATION

Prediction of a monolayer spin-spiral semiconductor: CoO with a honeycomb lattice

Jie Zhang(张杰)[1,2], Shunuo Song(宋姝诺)[1], Yan-Fang Zhang(张艳芳)[1,†], Yu-Yang Zhang(张余洋)[1], Sokrates T. Pantelides[3,1], and Shixuan Du(杜世萱)[1,2,4,‡]

[1] *Institute of Physics and University of Chinese Academy of Sciences, Chinese Academy of Sciences, Beijing* 100190, *China*
[2] *Beijing National Laboratory for Condensed Matter Physics, Beijing* 100190, *China*
[3] *Department of Physics and Astronomy and Department of Electrical and Computer Engineering, Vanderbilt University, Nashville, Tennessee* 37235, *USA*
[4] *Songshan Lake Materials Laboratory, Dongguan* 523808, *China*

(Received 5 April 2023; revised manuscript received 25 May 2023; accepted manuscript online 26 May 2023)

The recent successful fabrication of two-dimensional (2D) CoO with nanometer-thickness motivates us to investigate monolayer CoO due to possible magnetic properties induced by Co atoms. Here, we employ first-principles calculations to show that monolayer CoO is a 2D spin-spiral semiconductor with a honeycomb lattice. The calculated phonon dispersion reveals the monolayer's dynamical stability. Monolayer CoO exhibits a type-I spin-spiral magnetic ground state. The spin-spiral state and the direct bandgap character are both robust under biaxial compressive strain (−5%) to tensile strain (5%). The bandgap varies only slightly under either compressive or tensile strain up to 5%. These results suggest a potential for applications in spintronic devices and offer a new platform to explore magnetism in the 2D limit.

Keywords: spin-spiral semiconductor, type-II multiferroic, bandgap engineering, monolayer CoO

PACS: 75.85.+t, 75.70.Ak, 75.47.Lx, 75.50.Pp **DOI:** 10.1088/1674-1056/acd923

1. Introduction

Magnetic materials are used in information storage and other applications and are needed for the development of spintronics.[1,2] According to the Hohenberg–Mermin–Wagner theorem,[3,4] long-range magnetic ordering is prevented in isotropic two-dimensional (2D) materials at finite temperature due to thermal fluctuations. Nevertheless, the field of 2D magnetism has grown rapidly since the successful fabrication of 2D $FePS_3$ in 2016,[5,6] CrI_3[7] and $Cr_2Ge_2Te_6$ in 2017.[8] The past several years have witnessed a boost of 2D spin textures, such as skyrmions,[9] merons,[10] and spin spirals.[11] Spin-spiral materials, with a periodic modulated spin-rotating state, have received increasing interest. The long-range magnetic ordering breaks the space inversion symmetry, resulting in spontaneous electrical polarization. Thus, a spin-spiral system is also referred to as a type-II multiferroic, which is advantageous for magnetoelectric coupling in nanoelectronic devices. However, the only known 2D spin-spiral materials so far are $Hf_2VC_2F_2$,[12] $MnCl_2$,[13] Fe_3GeTe_2,[14] VOI_2,[15] NiI_2,[11,16] and FeOCl.[17] Among them, NiI_2 is the only one for which there exists experimental evidence of multiferroic behavior in the 2D limit. Due to the growing interest in the 2D spin-spiral field, it is appropriate to search for novel 2D spin-spiral materials.

Several 2D metal oxides (MOs) were recently reported to possess superior oxidation resistance, semiconductor character, and structural diversity.[18] In the last few years, there has been increasing interest in developing new fabrication methods for 2D MOs due to difficulties in synthesis[19–24] and also due to predictions of 2D MOs with intriguing properties.[18,25–28] Fabrication of a monolayer graphene-like ZnO membrane[29] and a square-lattice CuO membrane[30] residing in graphene pores has been reported. Recently, a 2D CoO nanosheet in a rock-salt structure was obtained from 3D nanocrystal intermediates,[20] while honeycomb CoO was derived from strictly controlled oxidation at the metal–gas interface.[31] The thicknesses of these two different 2D CoO materials are ∼ 1.0 nm and ∼ 0.84 nm, respectively. Bulk CoO is an antiferromagnetic insulator, exhibiting ferromagnetic spin alignment in each (111) plane and antiferromagnetic ordering between adjacent planes.[32,33] The top layer of the CoO(111) surface has a silicene-like honeycomb lattice. Therefore, it is worthwhile to explore the physical properties of monolayer CoO with a honeycomb lattice to give further guidance to experimental investigations and potential applications.

In this work, a single-atom-thick monolayer CoO is theoretically determined to be a stable spin-spiral material. Monolayer CoO has a planar honeycomb lattice in its equilibrium state. The calculated phonon dispersion confirms that monolayer CoO is dynamically stable. The electronic band structure shows that monolayer CoO is a direct-bandgap semiconductor

†Corresponding author. E-mail: zhangyanfang@ucas.ac.cn
‡Corresponding author. E-mail: sxdu@iphy.ac.cn

with a bandgap of 2.36 eV. Projected electronic band structures show that the out-of-plane d orbitals of Co atoms and p orbitals of O atoms contribute dominantly to the valence-band maximum (VBM), while the in-plane d orbitals and s orbitals of Co atoms together with the s orbitals of O atoms contribute dominantly to the conduction-band minimum (CBM). Remarkably, the spin-spiral ground state is robust under biaxial strains from -5% to 5%. Moreover, monolayer CoO remains a direct-bandgap semiconductor under biaxial strain.

2. Methods

In this work, geometric relaxations, total energy calculations, and electronic structure calculations were performed using density functional theory as implemented in the Vienna *ab initio* simulation package (VASP).[34,35] The spin-spiral calculation is conveniently modeled using the generalized Bloch theorem[36,37] without spin–orbital coupling (SOC). The magnetic ordering is calculated with SOC. The projector augmented-wave (PAW) method[38] and the generalized gradient approximation (GGA)[39] are used. To account for the localized 3d electrons of cobalt atoms, a Hubbard U correction ($U_{\text{eff}} = 5.1$ eV) is added to the Perdew–Burke–Ernzerhof (PBE) exchange–correlation functional based on Dudarev's approach.[40] The U_{eff} value is chosen because it results in a bandgap (2.5 eV) similar to the experimental value (2.5±0.3 eV) for bulk CoO.[41] The energy cutoff of the plane-wave basis set for all the calculations is 600 eV. The force convergence criterion is 0.001 eV/Å. The energy convergence criteria for the structure relaxation and self-consistent-field calculations are 10^{-6} eV and 10^{-8} eV, respectively. The vacuum region in each supercell in the z direction is 25 Å. The k-points sampling is Γ-centered, $18 \times 18 \times 1$ for the primitive cell, $6 \times 6 \times 1$ for the $3 \times 3 \times 1$ supercell, and $1 \times 1 \times 1$ for the $6 \times 6 \times 1$ supercell. The phonon dispersion is calculated using density-functional perturbation theory (DFPT) and post-processed in the PHONOPY code.[42] The polarization is calculated by the Berry-phase method.[43]

3. Results and discussion

A schematic of monolayer CoO with a planar configuration and a honeycomb lattice is shown in Fig. 1(a). The Co atoms form a hexagonal sublattice. The dynamic stability of this structure has been assessed by performing phonon-dispersion calculations. No imaginary frequency in the phonon dispersion is observed (Fig. 1(b)), suggesting that monolayer CoO is dynamically stable at 0 K.

Spin spirals are a periodic modulated spin-rotating state that is characterized by a propagation vector $\boldsymbol{q}$ representing the spin-rotating periodicity and direction. The relative total energy as a function of the propagation vector $\boldsymbol{q}$ based on spin-spiral calculations is used to evaluate the magnetic ground state of monolayer CoO, as shown in Fig. 2(a). The inset figure shows the Brillouin zone (BZ) and high-symmetry k points. Here, when the propagation vector has the same value as the Γ or M points in BZ, the spin spiral corresponds to a ferromagnetic (FM) or antiferromagnetic (AFM) ordering (Fig. 2(b)), respectively. The energy minimum occurs at $\boldsymbol{q} = (0.32, 0.32, 0)$, indicating a non-collinear spin-spiral magnetic ordering.

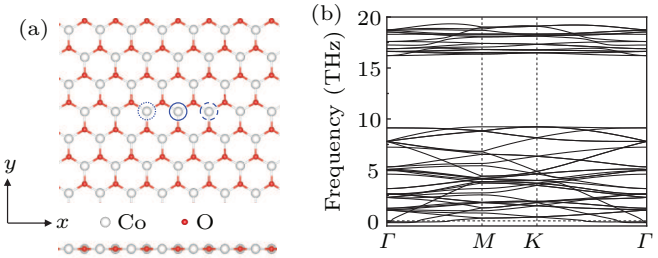

Fig. 1. Structure and stability of monolayer CoO. (a) Top and side views of monolayer CoO. White and red balls represent Co and O atoms, respectively. The dotted, solid-line, and dashed circles label the three nearest-neighboring Co atoms in the x direction which are analyzed in the strain-effect discussion, namely, Co_L, Co_M, and Co_R, respectively. (b) Phonon dispersion of monolayer CoO showing no imaginary frequencies.

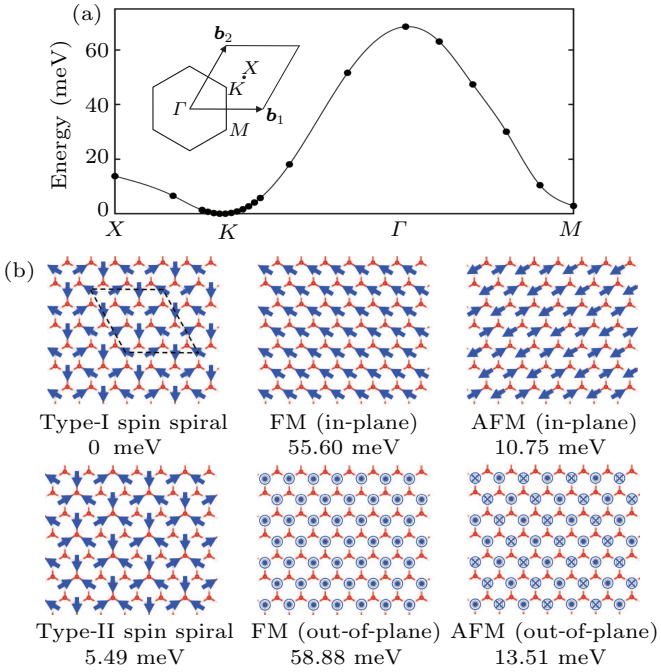

Fig. 2. Magnetic configurations of monolayer CoO. (a) The relative total-energy dependence on the propagation vector $\boldsymbol{q}$ for monolayer CoO. The inset figure shows the BZ with the reciprocal lattice vectors ($\boldsymbol{b_1}$ and $\boldsymbol{b_2}$) and three high-symmetry points, namely, Γ: (0, 0, 0), M: (0.5, 0, 0), and K: (1/3, 1/3, 0). The X-point coordinate is (0.5, 0.5, 0). The ground state (i.e., $\boldsymbol{q} = (0.32, 0.32, 0)$) is chosen as the reference. (b) Schematic top view of various magnetic configurations. Relative energies per formula are given at the bottom of each panel, with the spin-spiral and FM ordering obtained based on a $3 \times 3 \times 1$ supercell, while AFM ordering is based on a $2 \times 2 \times 1$ supercell. The energy of the type-I spin-spiral magnetic ordering is set to 0. Arrows, dots, and crosses represent spins in the plane, $+z$ direction, and $-z$ direction, respectively.

Figure 2(b) gives representative magnetic configurations with spin-spiral, FM, and AFM states. A $3 \times 3 \times 1$ supercell

(the dashed rhombus in Fig. 2(b)) is used to calculate the preferred spin-rotation plane of the spin-spiral state. Due to the absence of inversion symmetry, we considered in-plane type-I and type-II spin-spiral orderings (the left panel in Fig. 2(b)). The type-I spin-spiral ordering involves spins on three Co atoms in a hexagon pointing outwards from the center (the top figure), while the type-II spin-spiral ordering features spins on three neighboring Co atoms pointing towards the central O atom (the bottom figure). Taking into account spin–orbit coupling, the total energy of the type-I spin ordering is 5.49 meV per Co atom lower than that of the type-II spin ordering, suggesting that the spins rotate in a cycloidal manner around the z-axis.

The polarization induced by the type-I spin-spiral magnetic ordering is $(2.1, -1.2, 0)\times10^{-10}$ μC/cm. The polarization is totally in-plane. The magnitude is 2.4×10^{-10} μC/cm, which is one order of magnitude smaller than that of monolayer FeOCl.[17] We also considered in-plane and out-of-plane FM (AFM) magnetic orderings, as shown in the middle (right) panel of Fig. 2(b). We find that the in-plane spin ordering is more stable than the out-of-plane one for both FM and AFM magnetic configurations.

Dzyaloshinskii–Moriya interaction (DMI)[14,15,44] and magnetic frustration[12] are both possible origins for spin-spiral states. For MXene-like monolayer $Hf_2VC_2F_2$, the magnetism originates from the V atoms.[12] The in-plane V atoms form a triangular unit with AFM coupling between the nearest-neighboring V atoms, generating the 120° non-collinear Y-AFM ground state,[12] i.e., a spin-spiral magnetic ordering. Monolayer CoO is similar to the case of monolayer $Hf_2VC_2F_2$. The DMI interaction strength (0.5 meV) in monolayer CoO is weak compared with the exchange interaction strength (5.3 meV). The detail information about the calculation of the D and J values is shown in supplementary information. The AFM coupling indicated by the positive exchange interaction strength between the nearest-neighboring Co atoms, together with the triangle formed by nearest-neighboring Co atoms, leads to the spin-spiral magnetic ordering in monolayer CoO.

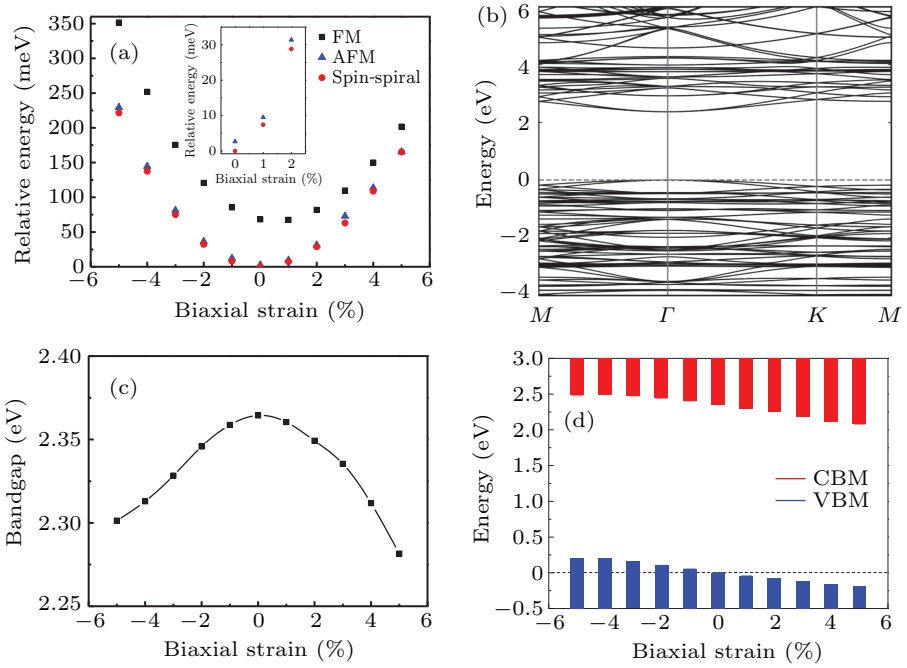

Fig. 3. Strain effect on the magnetic ground state and energy bands of monolayer CoO. (a) Relative energies of FM, AFM, and spin-spiral state as functions of the biaxial strain from −5% to 5% based on the unit cell. The inset figure shows a zoomed-in view of the relative energies with respect to the AFM and spin-spiral states from biaxial 0 to 2% tensile strain. (b) Energy bands of monolayer CoO at zero strain. (c) Bandgap variation from compressive strain to tensile strain (−5% to 5%). (d) Band-edge position distribution at various strains relative to the VBM position at zero strain, which is set to 0 eV (the dashed line).

Strains induced by the lattice mismatch between adlayers and the supporting substrates are inevitable during the growth of 2D materials and the fabrication of 2D-based devices.[45–50] Therefore, it is useful to evaluate the effect of strain on the magnetic configuration and the electronic structure of monolayer CoO. Here, we apply biaxial compressive and tensile strains from −5% to 5% by changing the lattice parameters and then relax the atomic positions, and obtain the energy bands from the relaxed configurations. By comparing the relative energies at FM, AFM, and spin-spiral magnetic states (Fig. 3(a)), it is found that the spin-spiral magnetic ground state is robust under strains less than 5%. The energy differences between the spin-spiral and the AFM states under 1% and 2% strains are 2 meV and 3 meV per formula (the inset in Fig. 3(a)), respectively. It is noteworthy that the energy difference between FM/AFM and spin-spiral state is generally on

the order of several meV.[16,17] Thus, the spin-spiral state is robust under strains less than 5%. Positive strain up to 5% induces only a very slight change in the spin-spiral propagation vector, from $\boldsymbol{q} = (0.32, 0.32, 0)$ to $\boldsymbol{q} = (0.31, 0.31, 0)$, while $\boldsymbol{q}$ remains at $(0.32, 0.32, 0)$ at compressive strains. However, strain shows the significant influence on the polarization of monolayer CoO. The polarizations are 7.7×10^{-10} μC/cm and 0.5×10^{-10} μC/cm under −4% compressive and 4% tensile strains, respectively. Comparing the polarization of monolayer CoO without strain, we find that the polarization values decrease from compressive to tensile strains.

The electron energy bands at the equilibrium spin-spiral state (zero strain) are plotted in Fig. 3(b). The CBM and VBM are both located at the Γ point, resulting in a direct bandgap (2.36 eV). From compressive strain (−5%) to tensile strain (5%), the bandgap first increases slightly from 2.30 eV, reaches a maximum value of 2.36 eV at zero strain, and then decreases to 2.28 eV, as shown in Fig. 3(c). The positions of the CBM and VBM remain at the Γ point over the entire strain range. Therefore, the direct bandgap character is well preserved. Figure 3(d) gives the band-edge position distribution under strains, referenced to the zero-strain VBM. The figure shows that the CBM position decreases slowly in the compressive strain region and more rapidly in the tensile strain region, while the VBM position decreases oppositely. This behavior is consistent with the bandgap variation.

To further explore the bandgap evolution behavior, the representative projected energy bands are plotted in Fig. 4. For a Co atom in the hexagonal sublattice (Co_M in Fig. 1(a)), there is one Co atom to the left (Co_L) and one to the right (Co_R) in the x direction. The projected band structures on the three Co atoms exhibit similar behavior. The CB mainly originates from the in-plane d orbitals of the Co atoms at compressive strain (Fig. 4(a)), while it originates from the s orbitals of the Co atoms at tensile strain (Fig. 4(c)). With the additional contribution from the Co s orbital, the band width of CB and CB+1 increases at tensile strain. From Fig. 4, we notice that the s orbitals of the O atoms contribute to the CBM at both compressive and tensile strains. Therefore, the orbital hybridization between Co and O changes from d_{xy}–s at compressive strain to s–s at tensile strain.

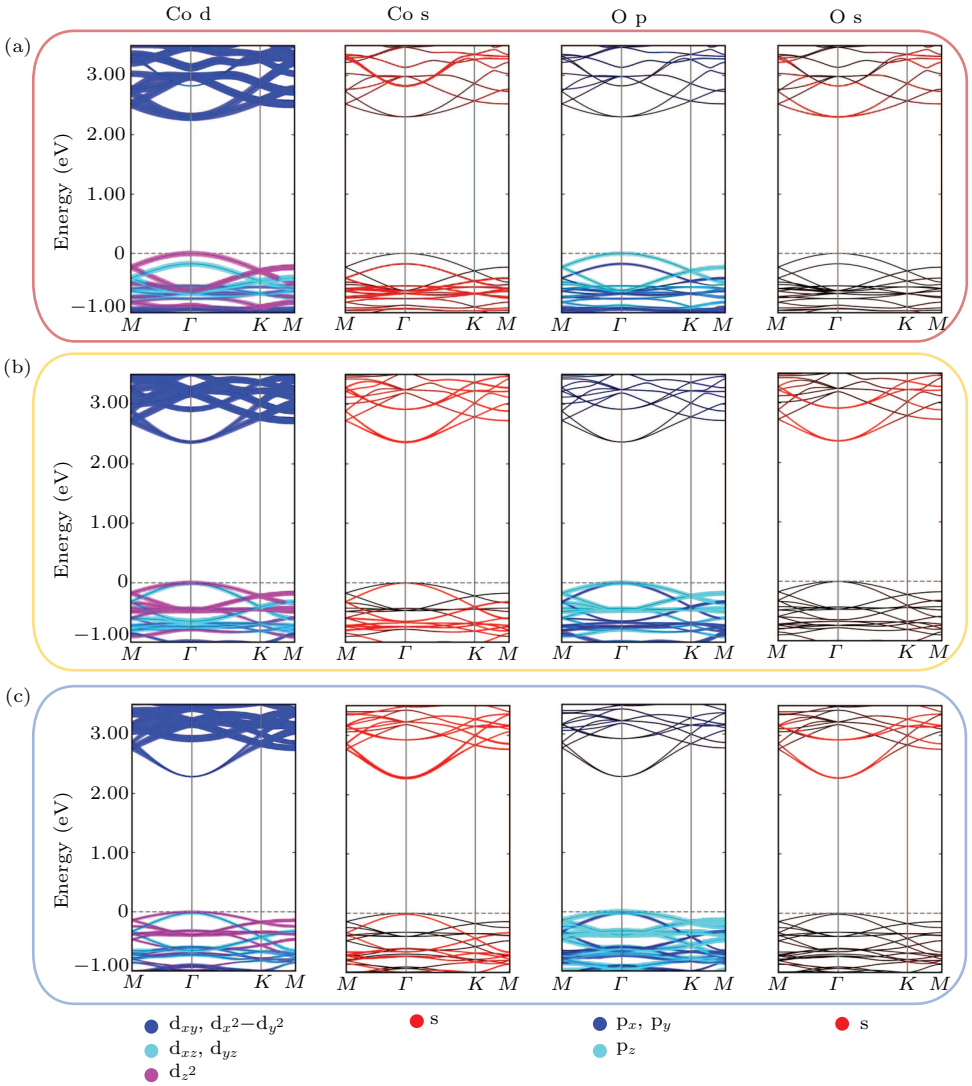

Fig. 4. Projected bands on the d and s orbitals of Co atoms and the p and s orbitals of O atoms under representative strains: (a) −5% compressive strain, (b) 0% at the equilibrium state, and (c) 5% tensile strain. The line width indicates the weight of the component.

In contrast, the VB is dominated by the out-of-plane d orbitals of the Co atoms. At Γ point, only the d_{z^2} orbitals contribute to the VBM at compressive strain, while both d_{z^2} and $d\pi$ orbitals contribute at tensile strain. Moreover, the p_z orbitals of the O atoms contribute to the VB at both compressive and tensile strains. The change of contribution indicates that the hybridization between d_{z^2} of Co and p_z of O decreases at tensile strain.

4. Conclusion and perspectives

In summary, we have demonstrated that monolayer CoO is a spin-spiral semiconductor with a 2.36 eV direct bandgap at the equilibrium state. The magnetic ground state of monolayer CoO is the in-plane type-I spin-spiral ordering with spins along the direction of the Co–O bond. The dynamic stability of the material is confirmed by the calculated phonon dispersion. It is found that the spin-spiral ground state and the direct bandgap character are both robust under biaxial strains from -5% to 5%. These findings bring monolayer CoO into the realm of 2D spin-spiral materials and can shed light on 2D magnetic metal-oxide nanomaterials for potential applications.

Acknowledgements

This work was supported by grants from the National Natural Science Foundation of China (Grant Nos. 52102193, 52250402, and 61888102), the Strategic Priority Research Program of the Chinese Academy of Sciences (Grant No. XDB30000000), and the Fundamental Research Funds for the Central Universities. Work at Vanderbilt was supported in part by the McMinn Endowment. Computational resources were provided by the National Supercomputing Center in Tianjin.

References

[1] Wolf S A, Awschalom D D, Buhrman R A, Daughton J M, von Molnár S, Roukes M L, Chtchelkanova A Y and Treger D M 2001 *Science* **294** 1488
[2] Han X F, Wan C H, Wu H, Guo C Y, Tang P, Yan Z R, Xing Y W, He W Q and Yu G Q 2022 *Chin. Phys. B* **31** 117504
[3] Mermin N D and Wagner H 1966 *Phys. Rev. Lett.* **17** 1133
[4] Hohenberg P C 1967 *Phys. Rev.* **158** 383
[5] Wang X Z, Du K Z, Liu Y Y F, Hu P, Zhang J, Zhang Q, Owen M H S, Lu X, Gan C K, Sengupta P, Kloc C and Xiong Q H 2016 *2D Mater.* **3** 031009
[6] Lee J U, Lee S, Ryoo J H, Kang S, Kim T Y, Kim P, Park C H, Park J G and Cheong H 2016 *Nano Lett.* **16** 7433
[7] Huang B V, Clark G, Navarro-Moratalla E, Klein D R, Cheng R, Seyler K L, Zhong D, Schmidgall E, McGuire M A, Cobden D H, Yao W, Xiao D, Jarillo-Herrero P and Xu X D 2017 *Nature* **546** 270
[8] Gong C, Li L, Li Z L, Ji H W, Stern A, Xia Y, Cao T, Bao W, Wang C Z, Wang Y, Qiu Z Q, Cava R J, Louie S G, Xia J and Zhang X 2017 *Nature* **546** 265
[9] Khanh N D, Nakajima T, Yu X Z, Gao S, Shibata K, Hirschberger M, Yamasaki Y, Sagayama H, Nakao H, Peng L C, Nakajima K, Takagi R, Arima T H, Tokura Y and Seki S 2020 *Nat. Nanotechnol.* **15** 444
[10] Augustin M, Jenkins S, Evans R F L, Novoselov K S and Santos E J G 2021 *Nat. Commun.* **12** 185
[11] Song Q, Occhialini C A, Ergeçen E, Ilyas B, Amoroso D, Barone P, Kapeghian J, Watanabe K, Taniguchi T, Botana A S, Picozzi S, Gedik N and Comin R 2022 *Nature* **602** 601
[12] Zhang J J, Lin L F, Zhang Y, Wu M H, Yakobson B I and Dong S 2018 *J. Am. Chem. Soc.* **140** 9768
[13] Prayitno T B and Ishii F 2019 *J. Phys. Soc. Jpn.* **88** 104705
[14] Laref S, Kim K W and Manchon A 2020 *Phys. Rev. B* **102** 060402
[15] Ding N, Chen J, Dong S and Stroppa A 2020 *Phys. Rev. B* **102** 165129
[16] Ni J Y, Li X Y, Amoroso D, He X, Feng J S, Kan E J, Picozzi S and Xiang H J 2021 *Phys. Rev. Lett.* **127** 247204
[17] Bao D L, O'Hara A, Du S X and Pantelides S T 2022 *Nano Lett.* **22** 3598
[18] Guo Y, Ma L, Mao K, Ju M G, Bai Y Z, Zhao J J and Zeng X C 2019 *Nanoscale Horiz.* **4** 592
[19] Zavabeti A, Ou J Z, Carey B J, Syed N, Orrell-Trigg R, Mayes E L H, Xu C L, Kavehei O, O'Mullane A P, Kaner R B, Kalantar-zadeh K and Daeneke T 2017 *Science* **358** 332
[20] Yang J, Zeng Z Y, Kang J, Betzler S, Czarnik C, Zhang X W, Ophus C, Yu C, Bustillo K, Pan M, Qiu J S, Wang L W and Zheng H M 2019 *Nat. Mater.* **18** 970
[21] Zhao S S, Zhang J Q and Fu L 2021 *Adv. Mater.* **33** 2005544
[22] Ta H Q, Mendes R G, Liu Y, Yang X Q, Luo J P, Bachmatiuk A, Gemming T, Zeng M Q, Fu L, Liu L J and Rümmeli M H 2021 *Adv. Sci.* **8** 2100619
[23] Chahal S, Kauzlarich S M and Kumar P 2021 *ACS Materials Lett.* **3** 631
[24] Xie H G, Li Z, Cheng L, Haidry A A, Tao J, Xu Y, Xu K and Ou J Z 2022 *iScience* **25** 103598
[25] Mounet N, Gibertini M, Schwaller P, Campi D, Merkys A, Marrazzo A, Sohier T, Castelli I E, Cepellotti A, Pizzi G and Marzari N 2018 *Nat. Nanotechnol.* **13** 246
[26] Yang T, Song T T, Callsen M, Zhou J, Chai J W, Feng Y P, Wang S J and Yang M 2019 *Adv. Mater. Interfaces* **6** 1801160
[27] Bandyopadhyay A, Frey N C, Jariwala D and Shenoy V B 2019 *Nano Lett.* **19** 7793
[28] Friedrich R, Ghorbani-Asl M, Curtarolo S and Krasheninnikov A V 2022 *Nano Lett.* **22** 989
[29] Quang H T, Bachmatiuk A, Dianat A, Ortmann F, Zhao J, Warner J H, Eckert J, Cunniberti G and Rümmeli M H 2015 *ACS Nano* **9** 11408
[30] Yin K B, Zhang Y Y, Zhou Y L, Sun L T, Chisholm M F, Pantelides S T and Zhou W 2017 *2D Mater.* **4** 011001
[31] Zhang B Y, Xu K, Yao Q F, Jannat A, Ren G H, Field M R, Wen X M, Zhou C H, Zavabeti A and Ou J Z 2021 *Nat. Mater.* **20** 1073
[32] Skomski R, Wei X H and Sellmyer D J 2008 *J. Appl. Phys.* **103** 07C908
[33] Deng H X, Li J B, Li S S, Xia J B, Walsh A and Wei S H 2010 *Appl. Phys. Lett.* **96** 162508
[34] Kresse G and Furthmüller J 1996 *Phys. Rev. B* **54** 11169
[35] Kresse G and Furthmüller J 1996 *Comput. Mater. Sci.* **6** 15
[36] Sandratskii L M and Guletskii P G 1986 *J. Phys. F: Met. Phys.* **16** L43
[37] Sandratskii L M 1991 *J. Phys.: Condens. Matter* **3** 8565
[38] Blöchl P E 1994 *Phys. Rev. B* **50** 17953
[39] Perdew J P, Burke K and Ernzerhof M 1996 *Phys. Rev. Lett.* **77** 3865
[40] Dudarev S L, Botton G A, Savrasov S Y, Humphreys C J and Sutton A P 1998 *Phys. Rev. B* **57** 1505
[41] van Elp J, Wieland J L, Eskes H, Kuiper P, Sawatzky G A, de Groot F M F and Turner T S 1991 *Phys. Rev. B* **44** 6090
[42] Togo A and Tanaka I 2015 *Scr. Mater.* **108** 1
[43] King-Smith R D and Vanderbilt D 1993 *Phys. Rev. B* **47** 1651
[44] Xu C S, Chen P, Tan H X, Yang Y R, Xiang H J and Bellaiche L 2020 *Phys. Rev. Lett.* **125** 037203
[45] Lin X, Lu J C, Shao Y, *et al.* 2017 *Nat. Mater.* **16** 717
[46] Dai Z H, Liu L Q and Zhang Z 2019 *Adv. Mater.* **31** 1805417
[47] Nguyen V H, Nguyen H V, Saint-Martin J and Dollfus P 2015 *Nanotechnology* **26** 115201
[48] Kramer E, van Dorp J, van Leeuwen R and Venstra W J 2015 *Appl. Phys. Lett.* **107** 091903
[49] Wang Y, Guo Y L, Zeng C X, Yang D Y, Zhang Y, Wu L T, Wu Y Z, Hao J, Wang J L and Yang R S 2022 *Nano Energy* **104** 107983
[50] Xian J J, Wang C, Nie J H, Li R, Han M J, Lin J H, Zhang W H, Liu Z Y, Zhang Z M, Miao M P, Yi Y F, Wu S W, Chen X D, Han J B, Xia Z C, Ji W and Fu Y S 2022 *Nat. Commun.* **13** 257